ACS APPLIED MATERIALS & INTERFACES

Research Article

www.acsami.org

Thermal and pH Responsive Polymer-Tethered Multifunctional Magnetic Nanoparticles for Targeted Delivery of Anticancer Drug

Banalata Sahoo,[†] K. Sanjana P. Devi,[‡] Rakesh Banerjee,[†] Tapas K. Maiti,[‡] Panchanan Pramanik,[†] and Dibakar Dhara*,[†]

[†]Department of Chemistry and [‡]Department of Biotechnology, Indian Institute of Technology Kharagpur, West Bengal 721302 India

Supporting Information

ABSTRACT: Targeted and efficient delivery of therapeutics to tumor cells is one of the key issues in cancer therapy. In the present work, we report a temperature and pH dual responsive core−shell nanoparticles comprising smart polymer shell coated on magnetic nanoparticles as an anticancer drug carrier and cancer cell-specific targeting agent. Magnetite nanoparticles (MNPs), prepared by a simple coprecipitation method, was surface modified by introducing amine groups using 3-aminopropyltriethoxysilane. Dual-responsive poly(*N*-isopropylacrylamide)-*block*-poly(acrylic acid) copolymer, synthesized by reversible addition-fragmentation chain transfer (RAFT) polymerization, was then attached to the amine-functionalized MNPs via EDC/NHS method. Further, to accomplish cancer-specific targeting properties, folic acid was tethered to the surface of the nanoparticles. Thereafter, rhodamine B isothiocyanate was conjugated to endow fluorescent property to the MNPs required for cellular imaging applications. The nanoparticles were characterized by X-ray diffraction (XRD), transmission electron microscopy (TEM), selected area electron diffraction (SAED), field emission scanning electron microscopy (FESEM), energy-dispersive X-ray spectroscopy (EDX), thermogravimetric analysis (TGA), zeta potential, vibrating sample magnetometer (VSM), X-ray photoelectron spectroscopy (XPS) measurements, and FTIR, UV−vis spectral analysis. Doxorubicin (DOX), an anticancer drug used for the present study, was loaded into the nanoparticles and its release behavior was subsequently studied. Result showed a sustained release of DOX preferentially at the desired lysosomal pH and temperature condition. The biological activity of the DOX-loaded MNPs was studied by MTT assay, fluorescence microscopy, and apoptosis. Intracellular-uptake studies revealed preferential uptake of these nanoparticles into cancer cells (HeLa cells) compared to normal fibroblast cells (L929 cells). The *in vitro* apoptosis study revealed that the DOX-loaded nanoparticles caused significant death to the HeLa cells. These nanoparticles were capable of target specific release of the loaded drug in response to pH and temperature and hence may serve as a potential drug carrier for *in vivo* applications.

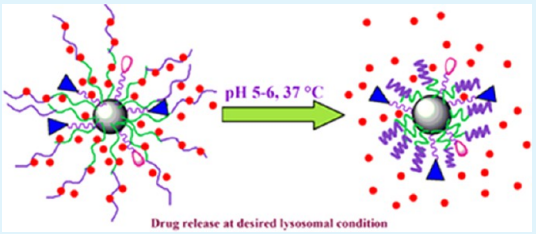

KEYWORDS: *magnetic nanoparticles, responsive block copolymers, doxorubicin, drug delivery, cancer cell targeting*

INTRODUCTION

Magnetic nanoparticles (MNPs) have gained significant attention for a myriad of biotechnological applications in recent years. Their biocompatibility and superparamagnetic nature render them suitable for diverse biological applications such as in drug and gene delivery,[1,2] contrast enhancement of magnetic resonance imaging,[3] tissue repair,[4] specific cell-detection,[5] hyperthermia,[6] magnetofection,[7] bioseparation,[8] and so on. Magnetic iron oxide, e.g., Fe_3O_4 nanoparticles are of great interest as vehicles for drug delivery because they can be suitably modified to carry drug molecules and be magnetically guided to the targeted organs or lesion sites inside the body. This helps in preventing the damage of normal organs or tissues due to drug toxicity even before reaching the targeted location,[9] thereby improving the therapeutic effect. Such applications necessitate uniformity of size and chemical stability of the nanoparticles, besides being dispersible in a liquid medium. Nonspecific targeting happens to be one of the major drawbacks of *in vivo* drug-delivery applications using MNPs thus making it necessary to engineer the nanoparticle-surface for successful target-specific drug delivery. Such targeting are especially important in the case of cancer therapies since most of the commonly used anticancer drugs, besides being expensive, may also lead to undesired side effects on healthy cells in case of unspecific action.[10] Introduction of specific antibodies or ligands helps the MNPs carrying the therapeutic agent to selectively bind and deliver the agent to the targeted cells via the receptor mediated endocytosis.[11] Among the various ligands explored, folic acid (FA), is one of the most promising candidates that has the potential for cancer-cell specific targeting[12] owing to the fact that FA has a high affinity for folate receptors (FRs) that are overexpressed in various human carcinomas, e.g., breast, ovary, lung, kidney, and others.[13−16] In fact, FA has received considerable attention as a targeting agent also due to its ability to conjugate with a wide

Received: February 13, 2013
Accepted: April 3, 2013
Published: April 3, 2013

variety of molecules, high stability, low cost, and non-immunogenicity.[17]

Over the past decade, nanoparticle-based drug delivery systems have shown a high degree of efficacy in cancer treatments due to their improved pharmacokinetics and biodistribution profiles via the enhanced permeability and retention (EPR) effect.[18] Although the EPR is effective in enhancing the accumulation of nanoparticles (NPs) within tumor tissues, the poor cellular internalization and insufficient drug release limits the dosages of anticancer drugs to levels below the optimum therapeutic value, thereby adversely affecting the efficacy of the chemotherapy treatment of cancer.[19] In order to address these issues, stimuli-responsive delivery systems have been explored to improve bioavailability of a drug.[20] Also, among the stimuli, pH-responsiveness is the most frequently investigated since pH values vary quite significantly in different tissues and cellular compartments.[21−23]

The extracellular environment of a tumor has a lower pH (~6.8) than blood and normal tissues (pH 7.4),[24−27] whereas those of late endosome and lysosome are even lower (~5.0−5.5).[28] Thus pH-sensitive delivery systems are of special interest in controlled drug-delivery as evident from the literature.[29] Among the other stimuli, heat is capable of affecting structural changes of a thermosensitive material resulting in release of entrapped molecules.[30−32] In this context, drug carriers based on a thermoresponsive polymer (exhibiting a lower critical solution temperature (LCST)) and magnetic nanoparticles (MNPs) capable of increasing the temperature locally have been reported.[33] Among the various interesting properties of MNPs that render them suitable in medical and biological applications, their capability to generate heat when an applied magnetic field is applied is an interesting phenomenon.[34] Hence, incorporation of MNPs in thermosensitive materials, also known as magnetothermally responsive materials,[35] seems to hold promise in cancer treatment as the remote application of AMF involves a conformational change of the polymer molecule forming an open-pore structure that may trigger the release of drugs.[36] Hence a magnetic nanoparticle containing pH and heat responsive material as well as having cancer-cell specific drug delivery and imaging capability would be of great interest.

In this study, we present a facile and efficient method to prepare MNPs of iron-oxide with surface modified by FA, dual-responsive block copolymer as well as rhodamine B isothiocyanate (RITC). Dual-responsive poly(*N*-isopropylacrylamide)-*block*-poly(acrylic acid) (PNIPA-*b*-PAA) was synthesized by reversible addition−fragmentation transfer (RAFT) polymerization and then covalently linked to the amine-functionalized nanoparticles. Thereafter, FA was tethered onto them through amide-bond formation to improve the cancer-cells specific targeting of the loaded drug. Further, RITC was attached to these FA and polymer-modified MNPs to endow a fluorescent property to the nanoparticles required for tracking cellular internalization of the MNPs. We further investigated the efficacy of these surface-modified nanoparticles toward cancer-cell specific targeted release of anticancer drug DOX. The biological activities of the DOX-loaded nanoparticles were evaluated by MTT assay, fluorescence microscopy, and apoptosis study.

EXPERIMENTAL SECTION

Materials. Anhydrous ferric chloride ($FeCl_3$), ferrous sulfate ($FeSO_4·7H_2O$), and ammonia solution (25−28%) were purchased from Merck. 3-Aminopropyl triethoxysilane (APTES), folic acid (FA), *N*-hydroxysuccinamide (NHS), 1-[3-(dimethylamino)propyl]-3-ethyl-carbodiimide hydrochloride (EDC), doxorubicin hydrochloride (DOX), rhodamine b isothiocyanate (RITC), 4′-6-diamidino-2-phenylindole (DAPI), propidium iodide (PI), RNase and 3-(4,5-dimethylthiazol-2-yl)-2,5-diphenyltetrazolium bromide (MTT), *N*-isopropylacrylamide (NIPA), *t*-butylacrylate, azobisisobutyronitrile (AIBN), trifluoroacetic acid were obtained from Sigma-Aldrich. Fetal bovine serum and Minimum Essential Medium (MEM) were obtained from Hyclone, USA and Himedia, India, respectively. *S*-1-Dodecyl-*S*′-(α,α′-dimethyl-α″-acetic acid) trithiocarbonate (CTA) was synthesized following a reported procedure.[37] Milli-Q water was used for all of the experiments.

Methods. *Preparation of Magnetic Iron Oxide (Fe_3O_4) Nanoparticles (MNPs).* Magnetic nanoparticles of Fe_3O_4, henceforth referred to as MNPs throughout this paper, were prepared by a chemical coprecipitation technique in aqueous medium according to a previously reported procedure.[38] In brief, a mixture of $FeCl_3$ (0.324 g) and $FeSO_4$ (0.278 g) in a 2:1 molar ratio were dissolved in 40 mL of Milli-Q water in a three-neck round-bottom flask equipped with a mechanical stirrer and argon atmosphere. To the above mixture, 5 mL of ammonium hydroxide was added dropwise and the solution was vigorously stirred at 80 °C. After stirring for an hour, the magnetite nanoparticles were recovered, washed thoroughly with Milli-Q water 3−4 times, and then dried.

Preparation of Amine-Functionalized MNPs (NH_2-MNPs). Amine functionalized MNPs (NH_2-MNPs) were prepared by grafting APTES by a sol−gel method. In a typical synthesis, 0.1 g of MNPs was first dispersed ultrasonically in 100 mL of 9:1 (v/v) ethanol−water mixture and 1 mL of ammonia solution for 30 min. To the above dispersed solution, 1 mL of APTES was added dropwise and the resulting mixture was stirred at room temperature for 12 h. Thereafter, the nanoparticles were magnetically concentrated, washed with ethanol properly, and then dried.

Synthesis of Poly(N-isopropylacrylamide)-block-poly(acrylic acid) (PNIPA-b-PAA). In the first step, *N*-isopropylacrylamide (NIPA) was polymerized to form a poly(*N*-isopropylacrylamide) macro chain transfer agent as follows. NIPA (0.565 g, 5.0 mmol), CTA (0.013 g, 0.05 mmol), AIBN (2.1 mg, 0.012 mmol), and dioxane (2.0 mL), were taken in a two-necked round bottom flask equipped with a magnetic stir bar and purged with nitrogen for 30 min. The reactor flask was then placed in a preheated oil-bath at 70 °C with constant stirring for 8 h. The reaction was then quenched by immersing the reactor in liquid nitrogen. Most of the dioxane was removed and the viscous materials was then dissolved in THF and precipitated from cold diethyl ether. The polymer was reprecipitated into ether and dried under vacuum at room temperature for 12 h to yield a yellow powder. The resulting polymer was characterized by ^{1}HNMR (400 MHz) and gel permeation chromatography. M_n of the polymer was determined by ^{1}HNMR as 7900 g mol^{-1}.

In the second step poly(*N*-isopropylacrylamide)-*block*-poly(*t*-butylacrylate) was prepared as follows. *tert*-Butyl acrylate (1.0 g, 7.81 mmol), poly(*N*-isopropylacrylamide) macro chain transfer agent (as prepared above) of M_n = 7900 g mol^{-1} and M_w/M_n = 1.10 (0.89 g, 0.11 mmol), AIBN (4.5 mg, 0.0275 mmol), and dioxane (4.0 mL) were taken in a two-necked round bottom flask and purged with nitrogen for 30 min. It was placed in a preheated oil-bath at 70 °C and stirred for 12 h. Thereafter, the polymerization was quenched by immersion of the reactor in liquid nitrogen. Dioxane was removed and the viscous product thus obtained was then dissolved in THF and precipitated from cold MeOH/H_2O (2:1) mixture, washed with MeOH, and dried to yield a yellow powder with M_n = 16 200 (^{1}HNMR), PDI = 1.23. The acrylic acid block was then produced by hydrolysis of the *t*-butyl acrylate block using trifluoroacetic acid treatment. The poly(*N*-isopropylacrylamide)-*block*-poly(*t*-butylacrylate) (1.50 g, 0.093 mmol) was dissolved in 20 mL of dry DCM, added trifluoroacetic acid (2.5 mL), and stirred for 14 h at room temperature (RT). The solvent was then removed and the polymer was redissolved in THF and precipitated from an ice-cold MeOH/H_2O (2:1) mixture, washed with MeOH, and finally dried to yield a

yellow powder with M_n = 13 308 (^{1}HNMR), PDI = 1.24. The cloud point of the resultant polymer (1.0 wt % solution) in aqueous solution of pH 8.0 was determined by monitoring the absorbance of the polymer solution at 500 nm at different temperatures, and it was found to be 34.0 °C. ^{1}HNMR spectra of poly(*N*-isopropylacrylamide)-*block*-poly(acrylic acid) and molecular weight data of the polymers are provided in the Supporting Information (see Figure S1 and Table S1 in the Supporting Information).

Preparation of PNIPA-b-PAA Modified Magnetic Nanoparticles (Poly-MNPs). The PNIPA-*b*-PAA was covalently linked to the NH_2-MNPs via the EDC/NHS method as follows. PNIPA-*b*-PAA (0.25 g) was dissolved in alkaline Milli-Q water. To this EDC (0.2 g) and NHS (0.2 g) were added, and the pH of the resulting solution was kept at 7.0−8.0 with dilute NaOH solution. The activation was carried at RT for 3−4 h. Then 0.05 g of aqueous dispersed aminated nanoparticles were added dropwise to the activated polymer solution, and the whole solution was stirred for 24 h at RT to form polymer modified magnetic nanoparticles (Poly-MNPs), which were eventually recovered through magnetic decantation, washed once again with Milli-Q water, and recovered.

Preparation of Folic Acid Tethered Polymer-Modified Magnetic Nanoparticles (FA-MNPs). Activation of the Poly-MNPs with FA was carried out via EDC/NHS chemistry according to a reported procedure with little modification.[39] In brief, 70.6 mg of FA (0.16 mmol) was dissolved in 10 mL of DMSO−Milli-Q water mixture (1:1 v/v) and the pH was maintained ∼8.0 by dilute NaOH solution. To the above FA solution, EDC (65.92 mg, 0.32 mmol) and NHS (36.83 mg, 0.32 mmol) were added and the pH of the mixture was maintained 7.0−8.0 by dilute NaOH. The FA activation was carried out for 4 h under dark conditions at RT. Thereafter, 50 mg of aqueous dispersion of Poly-MNPs was added dropwise to the activated FA solution, and the resulting mixture was stirred overnight in the dark at RT. Finally, the FA-modified Poly-MNPs (FA-MNPs) were magnetically precipitated, washed with water and DMSO several times, and finally recovered once again.

Preparation of Doxorubicin (DOX) Loaded FA-MNPs (DOX-MNPs). DOX was loaded into the FA-MNPs by the following method. In total, 10 mg of FA-MNPs were added to 10 mL of 0.3 mg/mL DOX solution and the mixture was kept in a shaker for 24 h in dark conditions. Finally, the DOX-loaded FA-MNPs (DOX-MNPs) were recovered by magnetic separation and washed twice with Milli-Q water to remove unbound drug molecules. The supernatant was collected to determine the drug loading content and drug encapsulation efficiency (EE) from UV−vis absorbance at 481 nm. The amount of DOX loaded into the nanoparticles was determined from a calibration curve obtained for a series of DOX solution at different concentrations. A representative picture of DOX loading in the nanoparticles is shown in Supporting Information (see Figure S2). The drug loading content and entrapment efficiency were determined by the following equations:

$$\text{drug loading contents (\%)} = \frac{\text{weight of drug in nanoparticles}}{\text{weight of nanoparticles taken}} \times 100$$

$$\text{drug entrapment efficiency (\%)} = \frac{\text{weight of drug in nanoparticles}}{\text{weight of drug injected}} \times 100$$

Preparation of RITC Labeled FA-MNPs (RITC-MNPs). A portion of the FA-MNPs prepared above were labeled with RITC, which is a highly fluorescent molecule. RITC was covalently linked to some of the free amine groups still present on the FA-MNPs. For this, 1 mg of RITC was dissolved in 2 mL of DMSO−Milli-Q water (1:1 v/v) mixture and the pH of this solution was adjusted to 8.0 with dilute NaOH. Then an aqueous suspension of 10 mg of FA-MNPs was added and stirred for 12 h in dark conditions at RT. The resulting RITC-labeled FA-MNPs (RITC-MNPs) were washed repeatedly to remove any unreacted or physically bound RITC molecules. Finally RITC-MNPs were recovered by magnetic precipitation and suspended in PBS buffer for further study. Similar labeling was also done on Poly-MNPs without folic acid modification (RITC-NFA-MNPs) in a similar manner as described and used as a control for an imaging study.

Nanoparticle Characterization Techniques. The phase purity and crystallinity of the MNPs and the Poly-MNPs were revealed by Phillips PW 1710 X-ray diffractometer (XRD) with Ni-filtered Cu−Kα radiation (l = 1.54 Å). The surface chemistry of nanoparticles was determined from FTIR spectra. Samples for FTIR spectra were prepared in KBr in the range 400−4000 cm^{-1}. The size and morphology of the nanoparticles were observed by high-resolution transmission electron microscopy (HRTEM) (JEOL 3010, Japan) operated at 300 kV. The nanoparticles were thoroughly dispersed in water by ultrasonication, and a drop of the solution was placed on a carbon coated copper grid and Phillips CM 200 was used for performing the field emission scanning electron microscopy (FESEM). The average particle size from TEM micrographs was analyzed using image J software. For the UV−vis absorption study of folic acid conjugation, drug loading, and release experiments, a Shimadzu absorption spectrophotometer (model no. UV-1700) was employed. The surface charge of the nanoparticles was investigated through zeta potential measurements (Zetasizer 4, Malvern Instruments, U.K.). Magnetic measurements of nanoparticles were performed using a SQUID-VSM instrument (Ever cool SQUID VSM DC Magnetometer). DLS measurements at different temperatures and pH were done using a Brookhaven 90 Plus particle size analyzer. Thermal analysis was done with a thermal analyzer (Pyris Diamond TG/DTA) with a heating rate 8 °C/min with a temperature range 50 to 1000 °C. Surface amine groups were quantified by TNBS assay according to the method reported in the Bioconjugate techniques book.[40] In brief, a particular amount of nanoparticles were dispersed in 0.1 M $NaHCO_3$ solution at pH 8.5. To this, 0.5 mL of 0.01% TNBS solution was added and mixed well and the whole solution was incubated at 37 °C for 2 h. After 2 h incubation, 0.5 mL of 10% SDS and 0.25 mL of 1 N HCl were added into this to stop the reaction. Then the whole solution was shaken well, and the UV−vis absorbance was taken at 335 nm. The above procedure was followed for the determination of amine groups present in glycine, which was used as the standard for determination of amine groups on the nanoparticle surface. The surface composition of nanoparticles was obtained from XPS analysis using an Al Kα excitation source in an ESCA-2000 Multilab apparatus (VG microtech) with a model Nexus-870, Thermo Nicolet Corporation, Wisconsin.

Drug Release Study. The cumulative drug release experiments were carried out at four different conditions to evaluate the stimuli-response behavior of the PNIPA-*b*-PAA toward pH and temperature. The release of DOX from the DOX-MNPs was carried out at physiological pH (pH ∼7.4) at 25 °C and at 37 °C. Similar studies were carried out at lysosomal pH condition (pH ∼5.5) at 25 °C and at 37 °C. For each experiment, 10 mg of DOX-MNPs were taken in 5 mL of phosphate buffer (pH ∼7.4) or in phosphate-citrate buffer (pH ∼5.5) and incubated in the above-mentioned temperature. The amount of released drug was checked spectrophotometrically (at 481 nm) at regular time intervals. The percentage of released drug was calculated from a standard curve of free drug solution.

Cell-Lines and Cytotoxicity Assay. *MTT Assay.* The biocompatibility of the FA-MNPs and DOX-MNPs was evaluated by standard MTT [3-(4,5-dimethylthiazol-2-yl)-2,5-diphenyltetrazolium bromide] assay. Two types of cells, namely, human cervical adeno carcinoma (HeLa) and normal fibroblast (L929) were acquired from the National Centre for Cell Sciences (NCCS), Pune, India. The cells were cultured in Minimum Essential Medium (MEM) or Dulbecco's Modified Eagle's medium (DMEM) supplemented with 10% fetal bovine serum, penicillin (100 units/ml), streptomycin (100 mg/mL), and 4 mM L-glutamine at 37 °C in tissue culture flasks with 5% CO_2 and 95% air humidified atmosphere. For experimental purposes, trypsinized cells were adjusted to a concentration of 1 × 10^5 cells/mL and plated in a 96 well flat bottom culture plate (180 μL/well). For toxicity studies, both cells were incubated with FA-MNPs and DOX-MNPs for 24 h at 37 °C in a humidified 5% CO_2 incubator. Then MTT was added and

cells were incubated. The resulting formazone crystals were solubilized by dissolving in an MTT solubilization buffer, the absorbance was measured at 570 nm by using a (Biorad) microplate reader, and the values were compared with respect to control cells.

Internalization of RITC-MNPs Using Fluorescence Microscopy Imaging. The internalization of RITC-MNPs and RITC-NFA-MNPs into both types of cells was observed by fluorescence microscope imaging. For intracellular uptake studies, 10 μg/mL of the nanoparticles of each type were incubated with folate receptor HeLa cells (FA(+)) and L929 cells (FA(−)) for 1 h and 4 h to determine the time dependent uptake of the nanoparticles. After incubation, cells were fixed with 4% paraformaldehyde for 15 min and stained with DAPI (1 mg/mL) for 10 min at 37 °C. Then cells were washed with PBS and observed under an Olympus IX 70 fluorescence microscope.

DAPI Staining for Nuclear Morphology Study. For visualization of HeLa cells, the nuclei of both the cells were stained with DAPI. The efficiency of DOX-MNPs was tested through apoptosis study. For this purpose, HeLa cells were treated with FA-MNPs (control set) and 10, 15, and 25 μg/mL DOX-MNPs for 24 h at 37 °C. Then, cells were fixed with 4% paraformaldehyde for 15 min, permeabilized with 0.1% Triton X-100, and stained with 1 mg/mL DAPI for 10 min. The cells were then rinsed with PBS and examined under fluorescence microscopy (Olympus IX 70).

RESULTS AND DISCUSSION

In this work, we have been able to design and prepare dual-responsive polymer-tethered multifunctional magnetic nanoparticles for targeted drug delivery of the anticancer drug doxorubicin (DOX). An illustration of the various steps involved in preparation of such tailored magnetic nanoparticles has been given in Scheme 1. As has been described earlier, the process involved preparation of magnetic iron oxide nanoparticles (MNPs) using aqueous coprecipitation approach in the very first step followed by grafting of APTES. Further, surface modification of the aminated iron oxide nanoparticles (NH_2-MNPs) were done through covalent linking of these functionalized MNPs successively with the dual-responsive PNIPA-*b*-PAA copolymers and folic acid via the EDC/NHS method resulting in Poly-MNPs and FA-MNPs, respectively. The portion of the polymer-tethered nanoparticles with or without FA was also labeled with RITC by covalent linking with some of the residual surface amine groups forming RITC-MNPs and RITC-NFA-MNPs, respectively.

Scheme 1. Proposed Schematic Presentation for the Designing of Polymer Modified Multifunctional Magnetic Nanoparticles

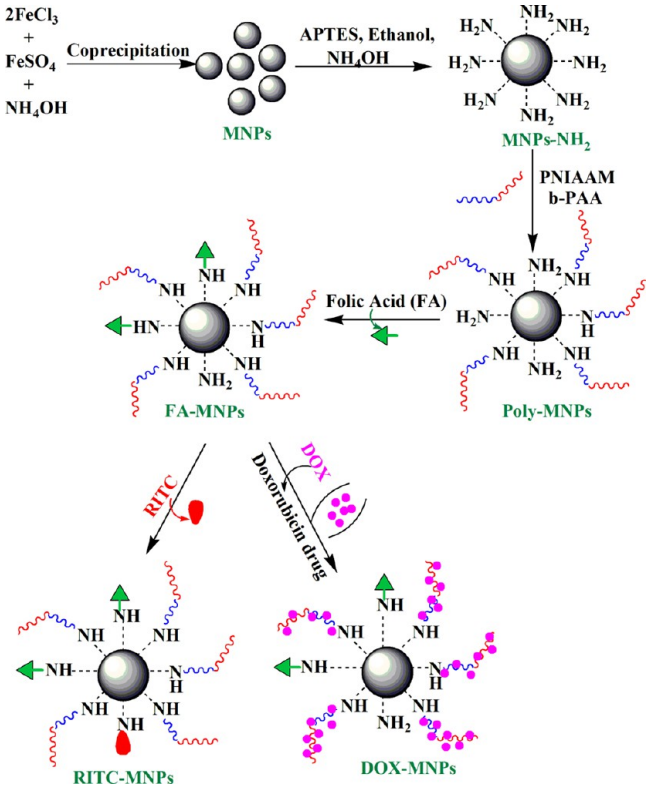

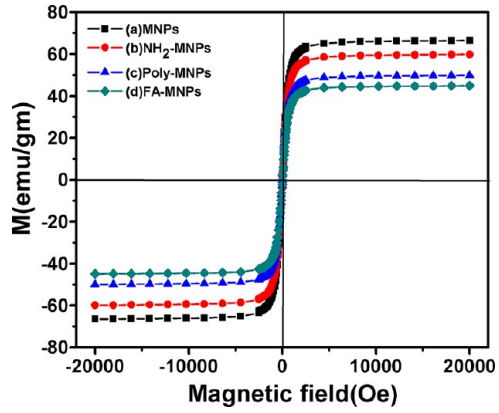

Figure 1. M-H curve for (a) MNPs, (b) NH_2-MNPs, (c) Poly-MNPs, and (d) FA-MNPs.

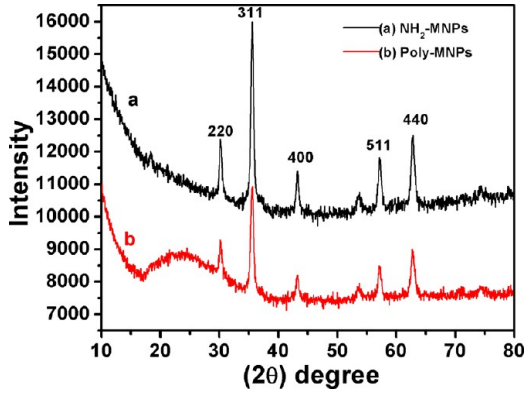

Figure 2. XRD pattern of (a) NH_2-MNPs and (b) Poly-MNPs.

Physicochemical Properties of Multifunctional Magnetic Nanoparticles. *Magnetic Measurements.* The magnetic properties of all the MNPs were studied by a superconducting quantum interference device (SQUID). The variations of magnetization value with applied magnetic field for various nanoparticles are displayed in Figure 1. From the magnetic curve, the particles showed superparamagnetic behavior at RT. The saturated magnetization values (Ms) for MNPs, NH_2-MNPs, Poly-MNPs, and FA-MNPs were calculated to be 66, 59, 48, and 44 emu/g, respectively. No coericivity and no remnant magnetization were observed in magnetic curve suggesting superparamagnetic nature of samples. A gradual decrease in the Ms values with surface modification was due to a decrease in the magnetic dipolar interaction with diamagnetic coating.[41] Despite the decrease in the magnetization value, the FA-MNPs still showed superparamagnetism and could be easily attracted by a magnet. This was evident from the fact that in every stage of nanoparticle preparation and subsequent surface modification, the nano-

dx.doi.org/10.1021/am400572b | ACS Appl. Mater. Interfaces 2013, 5, 3884−3893

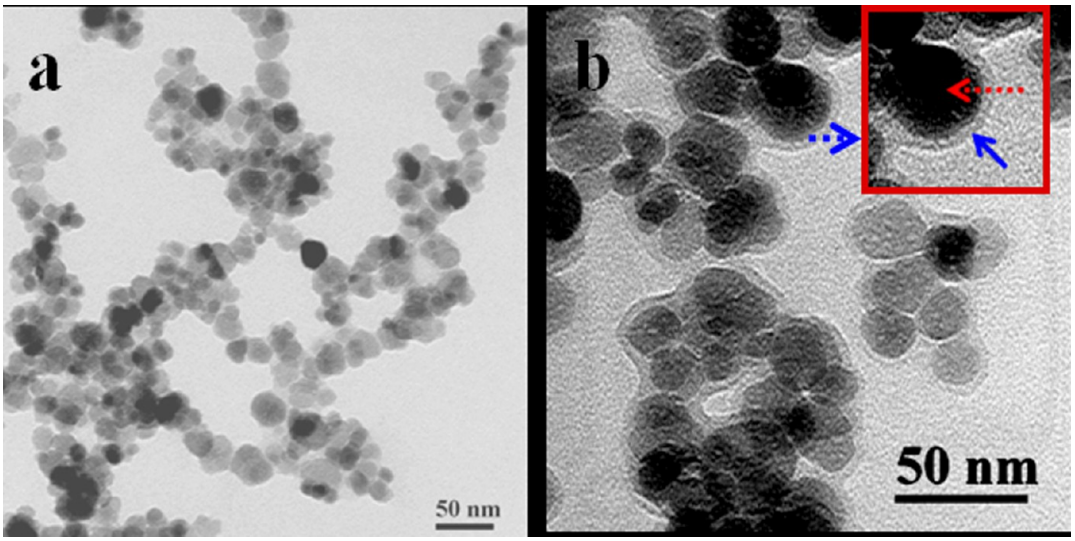

Figure 3. (a) TEM image of NH_2-MNPs and (b) high magnification TEM image of Poly-MNPs.

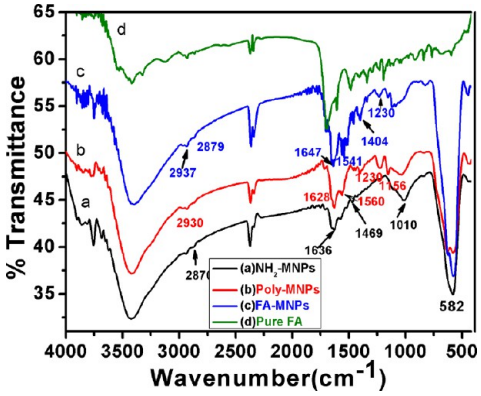

Figure 4. FTIR spectra of (a) NH_2-MNPs, (b) Poly-MNPs, (c) FA-MNPs, and (d) free FA.

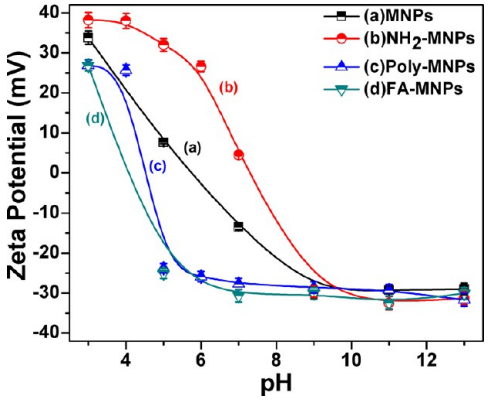

Figure 5. Zeta potential of (a) MNPs, (b) NH_2-MNPs, (c) Poly-MNPs, and (d) FA-MNPs.

particles were isolated from the aqueous dispersion by simple magnetic precipitation. From magnetic studies, it may be concluded that these FA-MNPs show high enough Ms values which have the potential to be used in magnet-guided drug delivery applications.

X-ray Diffraction Studies. The phase purity and crystalline nature of the prepared nanoparticles were ascertained by XRD analysis (Figure 2). The XRD pattern of NH_2-MNPs depicts

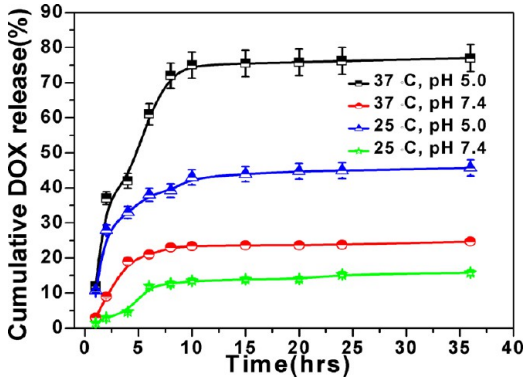

Figure 6. DOX release profile at different conditions from DOX-MNPs.

the usual peaks of pristine Fe_3O_4 nanoparticles. All the diffraction peaks in the diffraction pattern are well consistent with a standard JCPDS pattern (card no. 85-1436). An additional broad peak for the Poly-MNPs was observed at an angle between 20 and 30° due to amorphous polymer coating on the magnetite nanoparticles.

TEM and FESEM Study. The size and shape of these nanoparticles were observed by the TEM and FESEM study. The representative TEM images of NH_2-MNPs and Poly-MNPs are presented in Figure 3. Figure 3a shows that the nanoparticles were well dispersed, spherical in nature with an average particle size 20−25 nm. This size of the nanoparticles is well within the preferred range of the nanoparticles useful for effective drug-delivery.[42] The SAED pattern of above particles (see Figure S3a in Supporting Information) clearly show well-defined crystalline planes corresponding to an inner crystalline magnetic core. Low (see Figure S3b in Supporting Information) and high magnification TEM images of Poly-MNPs (Figure 3b) also reveal similar iron oxide nanoparticles coated with a polymer layer of thickness about 3.8 nm. Moreover, high-resolution TEM of Poly-MNPs shows a layer of polymer encapsulating on individual nanoparticles. One of the Poly-MNPs is shown in the inset of Figure 3b with higher magnification to clearly demonstrate the presence of the inner magnetic core with an outer polymer layer. The FESEM study

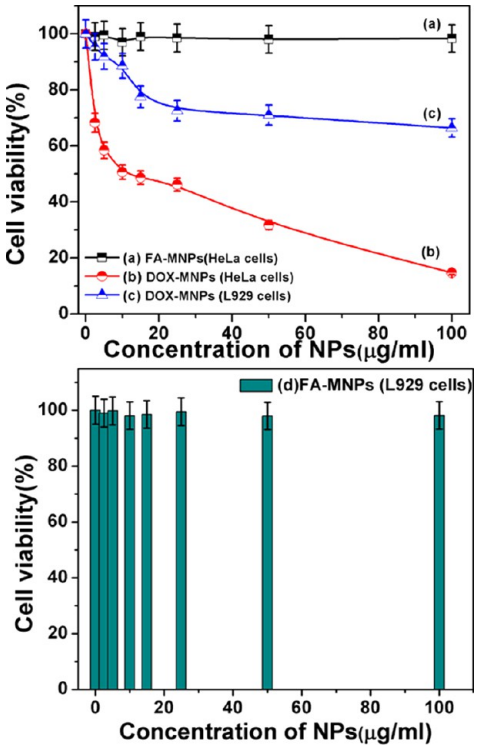

Figure 7. MTT assay of (a) FA-MNPs and (b) DOX-MNPs treated on HeLa cells, (c) DOX-MNPs treated on L929 cells, and (d) FA-MNPs treated on L929 cells.

of Poly-MNPs showed that the particles were very small with a nearly spherical shape (see Figure S4a in the Supporting Information). The elemental composition of Poly-MNPs contain Fe, O, C, N, Si, S elements as obtained from EDX analysis showing the successful polymer modification on the magnetic surface (see Figure S4b in the Supporting Information).

FTIR and UV–Visible Spectral Analysis. The presence of surface functional groups on nanoparticles was analyzed by FTIR analysis. FTIR spectra of NH_2-MNPs, Poly-MNPs, and FA-MNPs are shown in Figure 4. The spectra of NH_2-MNPs show peaks at 1636, 1469, 1010, 2870, and 582 cm^{-1}, which correspond to N–H bending, C–N stretching, Si–O–Si bond stretching, C–H bond vibration, and Fe–O bond vibration, respectively, demonstrating the aminosilane modification on Fe_3O_4 nanoparticles. After treatment with the block copolymer, two bands for amide bond vibration appeared at 1628 and 1560 cm^{-1} suggesting successful polymer modification on NH_2-MNPs. Additionally, for the Poly-MNPs, characteristic peaks of PNIPA-*b*-PAA polymer were observed at 1156, 1230, and 1404 cm^{-1} confirming the polymer linkage via an amide bond. FTIR of FA-MNPs shows all the characteristic peaks of folic acids revealing successful attachment of folic acid onto the Poly-MNPs. To further demonstrate the covalent linking of folic acid on Poly-MNPs, UV–vis spectral analysis was carried out. The UV–vis spectra of pure FA, FA-MNPs, and Poly-MNPs are shown in the Supporting Information, Figure S5. Pure FA showed two peaks at 280 and 360 nm due to n–π^* and π–π^* transitions, respectively.[43] After modification of Poly-MNPs, these two peaks were also observed with little shift convincing that the FA was successfully conjugated on the Poly-MNPs. Hence from XRD, FTIR, TEM, FESEM, Zeta potential, thermogravimetric analysis (TGA), and UV–vis spectra, the successive surface modifications by amine groups, polymer, and folic acid on iron oxide nanoparticles was confirmed.

DLS Measurements. DLS measurement of the dispersed Poly-MNPs was performed at various temperature and pH to monitor their temperature and pH dependent hydrodynamic volume. The hydrodynamic volume of the Poly-MNPs at pH 5.0 decreases near the LCST temperature of the PNIPA block copolymer and remained unchanged thereafter (see Figure S6a in the Supporting Information). This shows the temperature dependence of the polymer layer of the nanoparticles. This also confirms the LCST of the present block copolymers that are tethered on the MNPs is around 31 °C which is in well agreement with LCST of PNIPA.[44] The pH dependent hydrodynamic behavior was also noted by DLS measurement (see Figure S6b in the Supporting Information). The variation of hydrodynamic diameter of Poly-MNPs with both pH and temperature provides clear evidence for the formation of dual responsive core–shell magnetic nanoparticles.

Zeta Potential Measurements. The zeta-potential values for MNPs, NH_2-MNPs, Poly-MNPs, and FA-MNPs at various pHs are shown in Figure 5. The isoelectric point observed for MNPs was found to be a little above 6.0, which is close to the reported value of 6.5.[45] The shift of the isoelectric point to higher pH for NH_2-MNPs and to lower pH for Poly-MNPs suggest that the surface of the MNPs were modified by NH_2 groups, and subsequently, some of amine groups were functionalized and as a result free acrylic acid groups were present on the surface in the case of Poly-MNPs. The fact that zeta potential value of the Poly-MNPs abruptly changed to positive value below pH 5.0 which is near the pK_a value for carboxylic acid confirms the presence of acrylic acid groups. Below the pK_a, acrylic acid groups are present in the protonated form, hence the zeta potential of the nanoparticles are due to the protonated free amine groups present on the surface. A lower positive value for Poly-MNPs in comparison to NH_2-MNPs at low pH indicates that some of the free amine groups of NH_2-MNPs are not free in Poly-MNPs due to covalent attachment with the acrylic acid groups. A slightly more negative value of the zeta potential at higher pH for FA-MNPs was due to the introduction of additional carboxylic acids groups from folic acid.

The formation of the said surface-modified nanoparticles was further corroborated by TGA measurements. Step-wise weight loss at high temperature (Supporting Information, Figure S7) from the nanoparticles could be explained on the basis of decomposition of the surface functionalities introduced at various stages. We have also carried out amine quantification at different steps of surface modification. The results confirm the stepwise reduction in the amine group concentration on nanoparticles' surface as a result of modification by block copolymers and folic acid (see Table S2 in Supporting Information). Moreover, surface fictionalization was performed further and confirmed by XPS studies. A detail of XPS analysis and the data is given in Supporting Information (Figure S8).

In Vitro Drug Release. The loading content and entrapment efficiency of DOX in FA-MNPs are found to be 23.0% and 74.4%, respectively. The loading of DOX into the FA-MNPs is due to the electrostatic interaction between positive charged DOX molecules with the negatively charged PAA segment of the polymer chains.[46,47] The DOX loading amount in the polymeric shell observed here was found to be is much higher compared to DOX loading amount in other polymer shells as suggested in earlier reports.[48−50] *In vitro* DOX release from DOX-MNPs at different conditions is shown in Figure 6. The

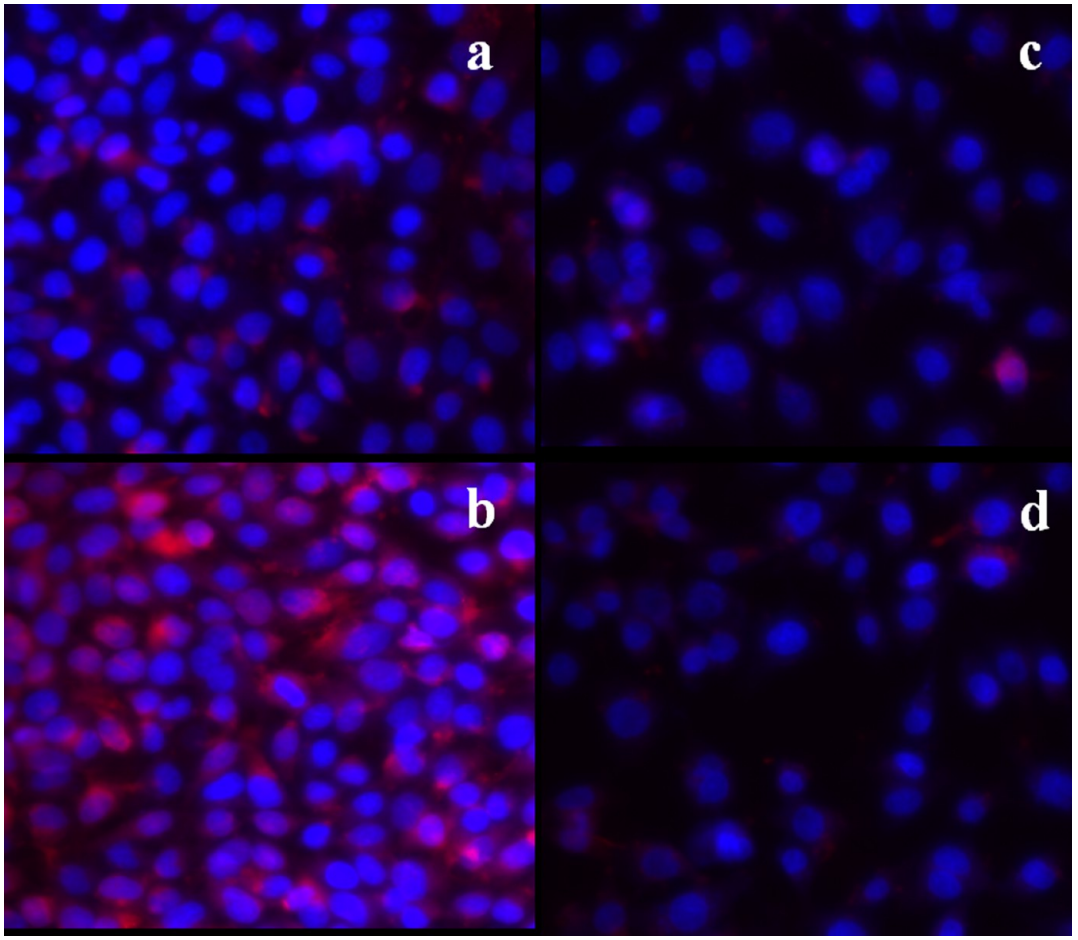

Figure 8. Fluorescence microscopy images of HeLa cells (left) and L929 cells (right) incubated with 10 μg/mL of RITC labeled FA-MNPs after 1 h (a and c) and 4 h (b and d) of incubation.

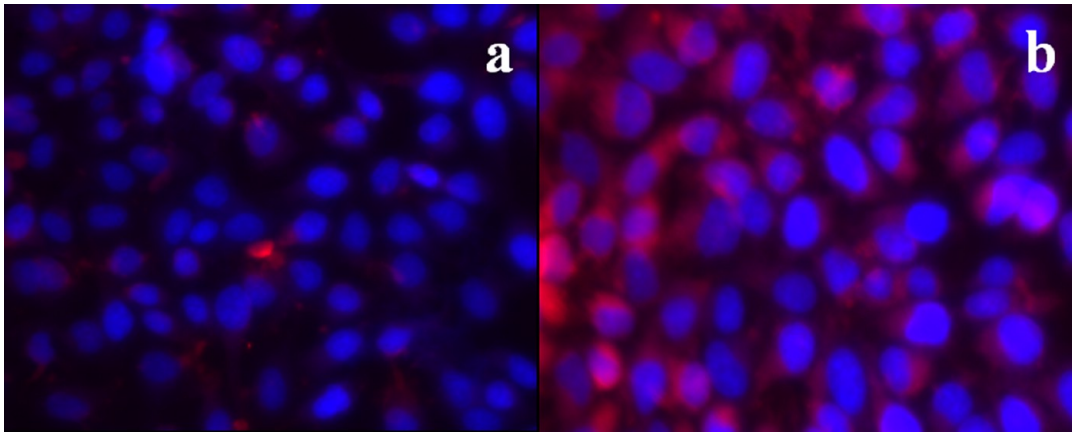

Figure 9. Intracellular uptake of RITC labeled MNPs into HeLa cells (a) without folate (RITC-NFA-MNPs) and (b) with folate (RITC-MNPs).

release performance was studied at both physiological and lysosomal pH conditions at temperatures 25 and 37 °C. The drug release profile revealed that the release rate was pH and temperature-dependent. About 75% of the loaded DOX was released after 10 h at pH 5.0 at 37 °C, whereas 42−43% drug was released at the same time interval at pH ∼5.0, 25 °C. The release rate was enhanced with an increase in temperature. The temperature responsive polymer played a key role for releasing more of the drug at 37 °C, the temperature inside the cell. Nearly, 23% DOX was released at pH 7.4 at 37 °C after 10 h. By contrast, after the same time duration, only 11−12% drug was released at pH 7.4 at 25 °C. For 37 °C, there is a drastic increase in the drug release amount and rate at pH 5.0 compared to pH 7.4. So the drug release pattern indicates the release amount and rate were dependent on pH and temperature, the best result was obtained for a pH-temperature combination that is prevalent in a cancer cell. At lower pH (pH 5.0) due to the protonation of carboxylic groups of the polymer block, the DOX-polymer interaction becomes weak and as a result DOX gets released at a much faster rate and in a larger

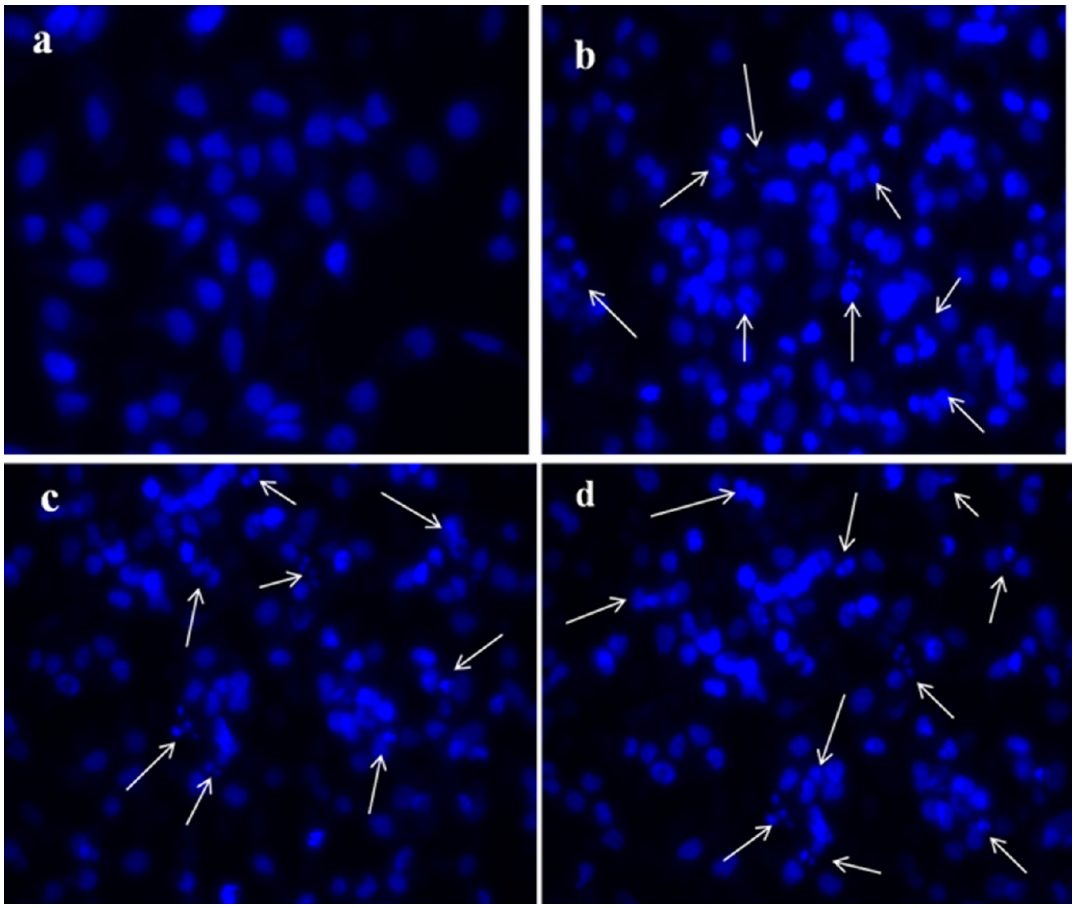

Figure 10. Apoptosis study of HeLa cells (a) treated with nanoparticles without DOX (FA-MNPs) and nanoparticles containing DOX (DOX-MNPs) (b) 10 μg/mL, (c) 15 μg/mL, and (d) 25 μg/mL.

amount. Again, the PNIPA block in the polymer shell shrinks at 37 °C, contributing to the facile release of the loaded drug. The drug release pattern indicated that the dual responsive block polymer played a key role on release of loaded drug in a desired fashion.

Biological Studies of Different Nanoparticles. *MTT Assay.* *In vitro* cytotoxicity of FA-MNPs and DOX-MNPs were studied on both HeLa cells and L929 cells by MTT assay. Figure 7 shows the cytotoxicity profile of L929 cells and HeLa cells incubated with various concentrations of FA-MNPs. These control nanoparticles without DOX caused no toxic effect on HeLa cells viability, and cells are viable up to 98% on treatment with 100 μg/mL of FA-MNPs. Particles were also nontoxic to L929 cells (shown in Figure 7d). Nearly 98% viable cells are observed after treatment with control nanoparticles. In contrast DOX-MNPs caused significant toxicity to both normal and HeLa cells. However, the effect was more pronounced in the case of HeLa cells. Normal L929 cells were alive up to 70% upon incubation with 100 μg/mL DOX-MNPs. However, the same drug loaded nanoparticles induced 84% killing of HeLa cells. IC_{50} value for HeLa cells was observed at a concentration of 10 μg/mL DOX-MNPs. The significant death of HeLa cells compared to L929 cells were due to receptor mediated endocytosis caused by folic acid. Hence MTT assay suggested that the folic acid conjugated polymer-tethered magnetic nanoparticles (FA-MNPs) were biocompatible to both types of cells, whereas the same set of nanoparticles with loaded anticancer drug (DOX-MNPs) preferentially inhibited the proliferation of HeLa cells.

Cellular Uptake Study. *In vitro* cellular internalization of nanoparticles was analyzed by fluorescence microscopy. HeLa (FR positive) and L929 (FR negative) cells were incubated with RITC-MNPs for two different durations, 1 and 4 h. The differential uptake behavior of both the types of cells is well evident from fluorescence images (shown in Figure 8). The nanoparticles were uptook more by HeLa cells than L929 cells via receptor (FA) mediated endocytosis. The fluorescence intensity increased with time as more nanoparticles were taken into the nuclei of HeLa cells. In contrast, a lower number of nanoparticles entered into L929 cells, suggesting that the RITC-MNPs preferentially targeted HeLa cells via receptor mediated targeting. Further, to verify the cancer specificity of the folate targeting moiety, fluorescence microscopy was done. For this purpose, HeLa cells were incubated with RITC-MNPs and RITC-NFA-MNPs for 4 h. As it can be clearly observed from Figure 9 that the presence of FA on nanoparticle surface resulted in easy internalization of the nanoparticles into HeLa cells compared to nanoparticles without FA. The presence of folic acid on the surface of the magnetic nanoparticles was also shown to enhance the internalization in FR(+) cells compared to the particles without folic acid on the surface by previous researchers.[51] Folic acid receptors are generally absent in most normal cells with few exceptions. Very low level of folate receptors are found in normal cells like choroid plexus, placenta, thyroid, and kidney.[52,53] The small size nanoparticles

uptake into normal cells mainly takes place through the endocytosis pathway, and for cancer cells the internalization mainly takes place through receptor mediated endocytosis.

Apoptosis Study. This study dealt with the synergistic effect of drug-loaded nanoparticles on proliferation of HeLa cells. DAPI staining of the nuclei for observation of nuclear morphology helps to distinguish the apoptotic nuclei from healthy ones. The apoptosis data is presented in Figure 10. When the control nanoparticles (FA-MNPs) were incubated with HeLa cells for 24 h, cell nuclei remained intact (Figure 10a). However, on treatment with different concentration of DOX-MNPs, there was significant nuclei fragmentation with condensed and apoptotic nuclei (Figure 10b–d). The concentration of apoptotic nuclei increased with an increase in drug-loaded nanoparticles (apoptotic nuclei shown by arrow in the figure). It has been reported that doxorubicin interacts with DNA topoisomerase II (topo II) causing the accumulation of enzyme-DNA adducts that ultimately lead to double-strand breaks and cell death via apoptosis.[54,55] Similar behavior of nuclei fragmentation was noticed by us when HeLa cells were treated with DOX-MNPs.

CONCLUSION

Polymer-tethered multifunctional magnetic iron oxide nanoparticles attached with fluorescent and targeting moieties was designed and prepared by a facile method. These were found to be potentially capable of temperature and pH responsive drug delivery specifically to cancer cells and also capable of cancer cell imaging. HRTEM images clearly showed magnetic nanoparticles coated with polymer shell of thickness 2.8–3.0 nm with the overall dimension of the resulting nanoparticles ~27–30 nm which is in desired size-range for drug delivery application. It was shown that these nanoparticles were taken up specifically by HeLa cancer cells in comparison to normal cells. Drug loading study indicated that the outer polymer shell encapsulate large amount of anticancer drug doxorubicin and release the anticancer drug preferably at pH 5.0 and temperature 37 °C. The loading content and entrapment efficiency reached as high as 23.0% and 74.4%, respectively. *In vitro* biological studies revealed that the doxorubicin-loaded folate-targeted nanoparticles achieved excellent efficacy for simultaneously targeting and destroying cancer cells. They specifically accumulate and release the payloads on HeLa cells through receptor mediated endocytosis. From all the biological studies, it is envisioned that these DOX-MNPs synthesized by us are excellent candidates that may serve as a vehicle in cancer-specific targeting, imaging, and therapeutic application in a single entity.

ASSOCIATED CONTENT

Supporting Information

^{1}HNMR of the polymer used for tethering with NH_2-MNPs, the molecular weights of the polymers synthesized in different steps, quantity of amine groups present on nanoparticle surfaces at the different stages of surface modification, picture of DOX loading, SAED pattern, FESEM, EDX, TGA, DLS, XPS analysis, and UV–vis spectral data of the nanoparticles. This material is available free of charge via the Internet at http://pubs.acs.org.

AUTHOR INFORMATION

Corresponding Author

*E-mail: dibakar@chem.iitkgp.ernet.in. Phone: +91-3222-282326. Fax: +91-3222-282252.

Notes

The authors declare no competing financial interest.

ACKNOWLEDGMENTS

Financial support from the Department of Science and Technology, Government of India, New Delhi, is acknowledged. B. Sahoo, K. Sanjana P. Devi, and R. Banerjee acknowledge CSIR, DBT, and UGC New Delhi, respectively, for their Research Fellowships.

REFERENCES

(1) Cao, S. W.; Zhu, Y. J.; Ma, M. Y.; Li, L.; Zhang, L. *J. Phys. Chem. C* **2008**, *112*, 1851–1856.
(2) Kievit, F. M.; Veiseh, O.; Fang, C.; Bhattarai, N.; Lee, D.; Ellenbogen, R. G.; Zhang, M. *ACS Nano* **2010**, *4*, 4587–4594.
(3) Xuan, S. H.; Lee, S. F.; Lau, J. T. F.; Zhu, X.; Wang, Y. X. J.; Wang, F.; Lai, J. M. Y.; Sham, K. W. Y.; Lo, P. C.; Yu, J. C.; Cheng, C. H. K.; Leung, K. C. F. *ACS Appl. Mater. Interfaces* **2012**, *4*, 2033–2040.
(4) Jenkins, S. I.; Pickard, M. R.; Granger, N.; Chari, D. M. *ACS Nano* **2011**, *5*, 6527–6538.
(5) Kaittanis, C.; Santra, S.; Perez, M. *J. Am. Chem. Soc.* **2009**, *131*, 12780–12791.
(6) Bae, K. H.; Park, M.; Do, M. J.; Lee, N.; Ryu, J. H.; Kim, G. W.; Kim, C.; Park, T. G.; Hyeon, T. *ACS Nano* **2012**, *6*, 5266–5273.
(7) Al-Deen, F. N.; Ho, J.; Selomulya, C.; Ma, C.; Coppel, R. *Langmuir* **2011**, *27*, 3703–3712.
(8) Tang, L.; Casas, J.; Venkataramasubramani, M. *Anal. Chem.* **2013**, *85*, 1431–1439.
(9) Zhang, J.; Lan, C. Q.; Post, M.; Simard, B.; Deslandes, Y.; Hsieh, T. H. *Cancer Genomics Proteomics* **2006**, *3*, 147–158.
(10) Wang, X.; Li, J.; Wang, Y.; Cho, K. J.; Kim, G.; Gjyrezi, A.; Koenig, L.; Giannakakou, P.; Shin, H. J. C.; Tighiouart, M.; Nie, S.; Chen, Z. G.; Shin, D. M. *ACS Nano* **2009**, *3*, 3165–3174.
(11) Yang, X.; Grailer, J. J.; Pilla, S.; Steeber, D. A.; Gong, S. *Bioconjugate Chem.* **2010**, *21*, 496–504.
(12) Yang, S. J.; Lin, F. H.; Tsai, K. C.; Wei, M. F.; Tsai, H. M.; Wong, J. M.; Shieh, M. J. *Bioconjugate Chem.* **2010**, *21*, 679–689.
(13) Yoo, M. K.; Park, I. K.; Lim, H. T.; Lee, S. J.; Jiang, H. L.; Kim, Y. K.; Choi, Y. J.; Cho, M. H.; Cho, C. S. *Acta Biomater.* **2012**, *8*, 3005–3013.
(14) Sudimack, J.; Lee, R. J. *Adv. Drug Delivery Rev.* **2000**, *41*, 147–162.
(15) Song, E. Q.; Zhang, Z. L.; Luo, Q. Y.; Lu, W.; Shi, Y. B.; Pang, D. W. *Clin. Chem.* **2009**, *55* (5), 955–963.
(16) Zhou, Y.; Wang, H.; Wang, C.; Li, Y.; Lu, W.; Chen, S.; Luo, J.; Jiang, Y.; Chen, J. *Mol. Pharmaceutics* **2012**, *9*, 1067–1076.
(17) Zhu, Y.; Fang, Y.; Kaskel, S. *J. Phys. Chem. C* **2010**, *114*, 16382–16388.
(18) Du, J. Z.; Du, X. J.; Mao, C. Q.; Wang, J. *J. Am. Chem. Soc.* **2011**, *133*, 17560–17563.
(19) Zhou, T.; Xiao, C.; Fan, J.; Chen, S.; Shen, J.; Wu, W.; Zhou, S. *Acta Biomater.* **2013**, *9*, 4546–4557.
(20) Zhu, Y.; Shi, J.; Shen, W.; Dong, X.; Feng, J.; Ruan, M.; Li, Y. *Angew. Chem., Int. Ed.* **2005**, *117*, 5213–5217.
(21) Chiang, W. H.; Ho, V. T.; Huang, W. C.; Huang, Y. F.; Chern, C. S.; Chiu, H. C. *Langmuir* **2012**, *28*, 15056–15064.
(22) Hua, D.; Jiang, J.; Kuang, L.; Jiang, J.; Zheng, W.; Liang, H. *Macromolecules* **2011**, *44*, 1298–1302.
(23) Liu, R.; Liao, P.; Liu, J.; Feng, P. *Langmuir* **2011**, *27*, 3095–3099.
(24) Gerweck, L. E.; Seetharaman, K. *Cancer Res.* **1996**, *56*, 1194–1198.

(25) Sun, H.; Guo, B.; Li, X.; Cheng, R.; Meng, F.; Liu, H.; Zhong, Z. *Biomacromolecules* **2010**, *11*, 848−854.
(26) Gao, W.; Chan, J. M.; Farokhzad, O. C. *Mol. Pharmaceutics* **2010**, *7*, 1913−1920.
(27) Wang, D.; Huan, X.; Zhu, L.; Liu, J.; Qiu, F.; Yan, D.; Zhu, X. *RSC Adv.* **2012**, *2*, 11953−11962.
(28) Hu, X.; Hao, X.; Wu, Y.; Zhang, J.; Zhang, X.; Wang, P. C.; Zou, G.; Liang, X. J. *J. Mater. Chem. B* **2013**, *1*, 1109−1118.
(29) Popat, A.; Liu, J.; Lu, G. Q. M.; Qiao, S. Z. *J. Mater. Chem.* **2012**, *22*, 11173−11178.
(30) Zhang, J. L.; Srivastava, R. S.; Misra, R. D. K. *Langmuir* **2007**, *23*, 6342−6351.
(31) Matsukuma, D.; Yamamoto, K.; Aoyagi, T. *Langmuir* **2006**, *22*, 5911−5915.
(32) Chen, S.; Li, Y.; Guo, C.; Wang, J.; Ma, J.; Liang, X.; Yang, L. R.; Liu, H. Z. *Langmuir* **2007**, *23*, 12669−12676.
(33) Louguet, S.; Rousseau, B.; Epherre, R.; Guidolin, N.; Goglio, G.; Mornet, S.; Duguet, E.; Lecommandoux, S.; Schatz, C. *Polym. Chem.* **2012**, *3*, 1408−1417.
(34) Yoo, D.; Lee, J. H.; Shin, T. H.; Cheon, J. *Acc. Chem. Res.* **2011**, *44*, 863−874.
(35) Brazel, C. S. *Pharm. Res.* **2009**, *26*, 644−656.
(36) Katagiri, K.; Imai, Y.; Koumoto, K. *J. Colloid Interface Sci.* **2011**, *361*, 109−114.
(37) Lai, J. T.; Filla, D.; Shea, R. *Macromolecules* **2002**, *35*, 6754−6756.
(38) Sahoo, B.; Sahu, S. K.; Bhattacharya, D.; Dhara, D.; Pramanik, P. *Colloids Surf. B* **2013**, *101*, 280−289.
(39) Singh, P.; Gupta, U.; Asthana, A.; Jain, N. K. *Bioconjugate Chem.* **2008**, *19*, 2239−2252.
(40) Hermanson, G. T. *Bioconjugate Techniques*, 2nd ed.; Academic Press: Boston, MA, 2008; p 128.
(41) Manju, S.; Sreenivasan, K. *Langmuir* **2011**, *27*, 14489−14496.
(42) Faraji, A. H.; Wipf, P. *Bioorg. Med. Chem.* **2009**, *17*, 2950−2962.
(43) Wu, H.; Liu, G.; Zhang, S.; Shi, J.; Zhang, L.; Chen, Y.; Chen, F.; Chena, H. *J. Mater. Chem.* **2011**, *21*, 3037−3045.
(44) Dhara, D.; Chatterji, P. R. *Langmuir* **1999**, *15*, 930−935.
(45) Parks, G. A. *Chem. Rev.* **1965**, *65*, 177−198.
(46) Ma, W. F.; Wu, K. Y.; Tang, J.; Li, D.; Wei, C.; Guo, J.; Wang, S. L.; Wang, C. C. *J. Mater. Chem.* **2012**, *22*, 15206−15214.
(47) Pan, Y. J.; Chen, Y. Y.; Wang, D. R.; Wei, C.; Guo, J.; Lu, D. R.; Chu, C. C.; Wang, C. C. *Biomaterials* **2012**, *33*, 6570−6579.
(48) Yang, J.; Lee, C. H.; Ko, H. J.; Suh, J. S.; Yoon, H. G.; Lee, K.; Huh, Y. M.; Haam, S. *Angew. Chem., Int. Ed.* **2007**, *46*, 8836−8839.
(49) Yang, X.; Grailer, J. J.; Rowland, I. J.; Javadi, A.; Hurley, S. A.; Matson, V. Z.; Steeber, D. A.; Gong, S. *ACS Nano* **2010**, *4*, 6805−6817.
(50) Kwon, G.; Naito, M.; Yokoyama, M.; Okano, T.; Sakurai, Y.; Kataoka, K. *J. Controlled Release* **1997**, *48*, 195−201.
(51) Ke, J. H.; Lin, J. J.; Carey, J. R.; Chen, J. S.; Chen, C. Y.; Wang, L. F. *Biomaterials* **2010**, *31*, 1707−1715.
(52) Wang, S.; Low, P. S. *J. Controlled Release* **1998**, *53*, 39−48.
(53) Sudimack, J.; Lee, R. J. *Adv. Drug Delivery Rev.* **2000**, *41*, 147−162.
(54) Bodley, A.; Liu, L. F.; Israel, M. *Cancer Res.* **1989**, *49*, 5969−5978.
(55) Cowell, I. G.; Okorokov, A. L.; Cutts, S. A.; Padget, K.; Bell, M.; Milner, J.; Austin, C. A. *Exp. Cell Res.* **2000**, *255*, 86−94.